RSC Sustainability

ROYAL SOCIETY OF CHEMISTRY

PAPER

View Article Online
View Journal | View Issue

Cite this: *RSC Sustainability*, 2024, **2**, 3375

Using waste to treat waste: efficient alcoholysis of PET waste with a shrimp shell derived catalyst using the response surface method†

Ruiyang Wen, Guoliang Shen, * Meiqi Zhang, Lejia Yang, Linlin Zhao, Haichen Wang and Xingzhu Han

Received 16th August 2024
Accepted 17th September 2024

DOI: 10.1039/d4su00487f

rsc.li/rscsus

The recycling of post-consumer PET is a significant area of scientific research, with great importance for resource recycling and environmental protection. Here, we present our work on the glycolytic depolymerization of post-consumer PET, and we utilized kitchen waste shrimp shells as a raw material to prepare a derivative catalyst. To optimize the reaction in terms of PET conversion and BHET yield, the RSM based on the Box–Behnken design was applied for the process of the reaction. Based on the experimental results, regression models as a function of significant process parameters were obtained and evaluated by ANOVA to predict the depolymerization performance of X-700; the conversion of PET is 100% and the yield of BHET is 80.84% under the optimization conditions by the RSM. The yield of BHET still reached 76.30% after 3 cycles. The catalyst offers several advantages, including superior catalytic activity, low cost, environmental friendliness, a simple preparation method, and reusability. These advantages can provide valuable references for the preparation of biomass catalysts and their application in polymer waste.

Sustainability spotlight

The effective management of solid waste is a crucial aspect of achieving carbon-neutral environmental protection. The conversion of waste PET into high-value-added fine chemicals not only mitigates environmental pollution and CO_2 emissions but also indirectly safeguards petroleum resources. Moreover, seafood restaurant waste is a rich source of various metal elements, and burial and incineration are suboptimal disposal methods. This study presents the development of a reusable metal catalyst derived from discarded shrimp shells, which further closes the resource loop by utilizing PET for open degradation. This work sustainability highlights the importance of UN sustainable development goals sustainable cities and communities (SDG 11), responsible consumption and production (SDG 12), and climate action (SDG 13).

1 Introduction

In response to global climate change, achieving carbon neutrality by 2050 is the most pressing task of our society nowadays. To this end, it is of utmost importance and a significant challenge to improve the efficiency of energy and reduce carbon emissions. For the current carbon emissions, a part of it comes from the combustion of polymer waste.[1,2] Polyester plastic (PET) is a widely used material due to its light weight, excellent mechanical properties, and low cost. It is the most cost-effective thermoplastic polymer material used in the fiber manufacturing, packaging, and textile industries.[3,4] PET consumption has increased over the years, with an estimated annual usage of approximately 70 million barrels of oil for processing virgin polyester fibers. Regrettably, the global recycling rate for PET waste is less than 10%.[5] PET's excellent stability makes it difficult to degrade in nature, exacerbating environmental pressures and creating a serious global issue. PET recycling is a crucial step towards addressing resource and environmental concerns. Chemical recovery is considered the most environmentally friendly method for PET treatment among many options. This method avoids the degradation of plastic properties that can occur with multiple cycles. Recently, there has been significant interest in developing a process for converting waste PET into monomers. Currently, the chemical recovery method has developed various processes, including dialysis,[6,7] monohydric alcoholysis,[8,9] ammonolysis,[10,11] and hydrolysis.[12,13] These processes can obtain high-quality monomers for further chemical reactions. Ethylene glycol can be used as a reactant for the synthesis of PET, as well as a reaction solvent and reactant for depolymerizing PET to obtain a BHET monomer with higher purity. This process avoids introducing impurities into the system, and the resulting BHET can be repolymerized to produce a product comparable to the original

School of Petrochemical Engineering, Shenyang University of Technology, Liaoyang, 111003, China. E-mail: shengl_shxy@sut.edu.cn

† Electronic supplementary information (ESI) available. See DOI: https://doi.org/10.1039/d4su00487f

PET. These advantages make ethylene glycol degraded PET a standout option for PET recovery.[14,15]

Currently, there is extensive research on catalysts for the alcoholysis of PET, including metal oxides, metal salts, molecular sieves, alkalis, and organic and ionic liquid catalysts have been developed and explored.[16–20] However, these catalysts are expensive to prepare, and finding lower-cost alternatives is a current research focus. Prof. Yan Ning reviewed the high value-added utilization methods of seafood waste, including extracting protein, calcium carbonate and chitin from it.[21,22] Several studies have demonstrated that catalysts derived from biomass, such as those made from lignin derivatives, eggshells, and seafood shells, exhibit significant catalytic activity in the PET depolymerization process to BHET.[23–25] Shrimp shells as a common and abundant seafood kitchen waste, which are particularly rich in metal elements. Although the main treatment methods for shrimp shells are landfill and composting, these methods do not fully exploit their chemical reuse value. Presently, shrimp shells have been subjected to a variety of high-value material treatments, including solution chemical treatment, hydrothermal treatment, and carbonization. There are several previous studies pertinent to the transformation of shrimp shells into carbon materials.[26–28] Their applications in catalysis, adsorption, sensing, and polymer additives have garnered considerable attention.[29–31] After undergoing pyrolysis, the material can be utilized as a natural metal-doped catalyst for further investigation into its potential applications in chemical reactions. For example, Yan used chitin extracted from shrimp shells as the raw material and prepared N-containing carbon materials derived through carbonization, and systematically studied the relationship between the structure and the carbonization temperature. The finally obtained materials showed excellent performance in heavy ion adsorption in water and epoxidation of styrene.[32]

Herein, this work utilized shrimp shell derivatives as catalysts for PET alcoholysis, following the green chemistry concept of waste management. To optimize the reaction parameters of the depolymerization process and the Box–Behnken experimental design, the RSM method could make the reaction easier to draw the functional relationship between variables and results.[33–35] The study demonstrates an effective method for the recycling of food waste and the high value-added recycling of waste PET plastics.

2 Materials section

2.1 Preparation of the catalyst

The shrimp shells were heated at 300 °C for 6 h, ground to a powder at room temperature, soaked in a 1% sodium hydroxide solution for 3 h, washed with deionized water and anhydrous ethanol, and dried at 100 °C for 3 hours. Subsequently, they were calcined at 500 °C, 600 °C, and 700 °C for 6 h in an N_2 atmosphere, and named X-500, X-600, and X-700 (Fig. 1).

2.2 Glycolysis of PET waste

The PET sheet, EG, and X catalyst (weighed by using PET mass) were added into a 100 ml round-bottom flask equipped with a thermometer and a reflux condenser. The flask was placed in an oil bath at 190–200 °C for an atmospheric pressure reaction. After the reaction, deionized water was added to the reaction substrate to reach a constant volume of 150 ml. The catalyst and product were separated using three vacuum filtrations: (1) the above-mixed system was vacuum filtered at 45 °C. The BHET product was obtained by placing the filtrate in a refrigerator at 5 °C for 12 h and then vacuum filtering it. (2) The residue on the filter paper was dissolved in deionized water at 80 °C, and vacuum filtration was carried out at this temperature to separate and recycle the catalyst. (3) The filtrate from step (2) was refrigerated at 5 °C for 12 h. After vacuum filtration, the product on the filter paper was dried to obtain oligomer L-PET, which includes the PET dimer and trimer. The experiment's overall flow chart is presented in Fig. 2.

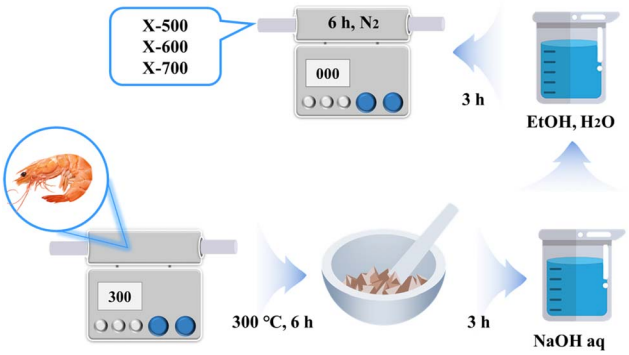

Fig. 1 Preparation of the shrimp shell derivative catalyst.

2.3 Responsive surface design

The RSM design employs a reliable experimental design and collects data through experiments. It fits the functional relationship between factors and response values using a multivariate quadratic regression equation and solves various variable problems using statistical methods. This method is widely used in chemical processes due to its convenience and ability to present data effectively. Our research group has published research results in recent years that demonstrate the convenience of response surface methods for PET degradation, based on the design of response surface experiments and their application.[5,14,33,34]

Design-Expert software version 13.0 was used to process the experimental data of PET degradation, and the yield of BHET was studied using the Box–Behnken design. Table 1 shows the complete response surface factor coding values (the level range of each single factor was determined by a single factor experiment, as shown in Fig. S3 in the ESI†).

3 Results and discussion

3.1 Characterization of the catalyst

FT-IR was used to characterize the functional group structure of the three catalysts in the range of 4000–400 cm^{-1}. The vibration band at 3637.2 cm^{-1} is attributed to the vibration peak of free-OH, indicating the presence of free-OH at calcination

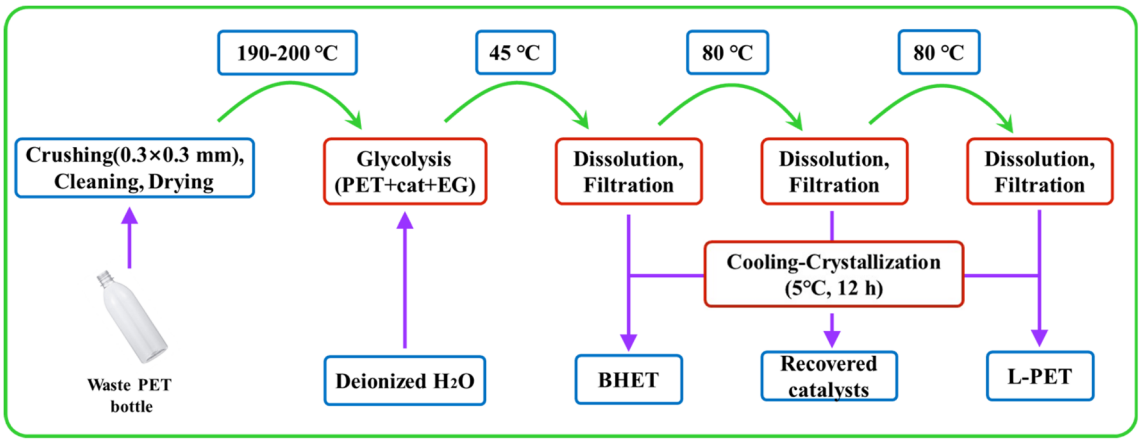

Fig. 2 The operation steps of the experiment.

Table 1 Levels of independent variables used for optimization

		Coded and actual values		
Independent variable	Unit	−1	0	1
A: time	h	2	3	4
B: temperature	°C	190	195	200
C: catalyst dosage	%	0.50	0.75	1.00
D: EG volume	ml	10	12	14

temperatures of ≥600 °C, but not at 500 °C. Additionally, 1423.3 cm^{-1} and 1026.5 cm^{-1} are the stretching vibration peaks of C–O. As the calcination temperature increases, the peak intensity gradually decreases, indicating that heating causes C–O fracture and weakens the C–O structure in the catalyst. The vibration peak at 877.1 cm^{-1} is caused by the in-plane bending vibration of CO_3^{2-}. Similar to C–O, the peak intensity of CO_3^{2-} also gradually weakens with increasing calcination temperature of the catalyst. This indicates that the catalyst structure changes from the ionic bond of CO_3^{2-} salt to other chemical bond binding modes as the calcination temperature increases. The vibration peak at 560.1 cm^{-1} and surrounding frequencies are caused by the vibration of M–O in the catalyst (M represents metal) (Fig. 3).

The XRD pattern of the X-500, 600, and 700 catalyst shows sharp peaks, indicating that it is a multi-component mixed system catalyst. The diffraction peaks at 2θ = 25.87°, 31.74°, 32.86°, 34.04°, and 45.30° correspond to the (002), (211), (300), (202), and (203) crystal planes of the PDF·# 73-0294 standard card, respectively. The catalyst sample contains $Ca_5(PO_4)_3(OH)$. The diffraction peaks observed at 2θ = 29.40°, 35.97°, and 47.52° correspond to the (104), (110), and (018) crystal planes of the PDF·# 83-0578 standard card, respectively. These peaks indicate the presence of $CaCO_3$ in the sample. Additionally, the diffraction peaks observed at 2θ = 17.79° and 46.60° correspond to the (001) and (011) crystal planes of the PDF·# 84-1275 standard card. The presence of $Ca(OH)_2$ in the sample causes

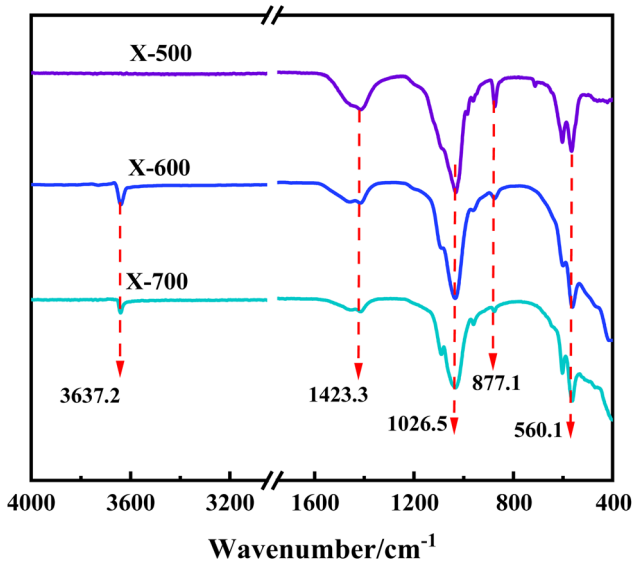

Fig. 3 FT-IR spectra of X-500, 600, and 700.

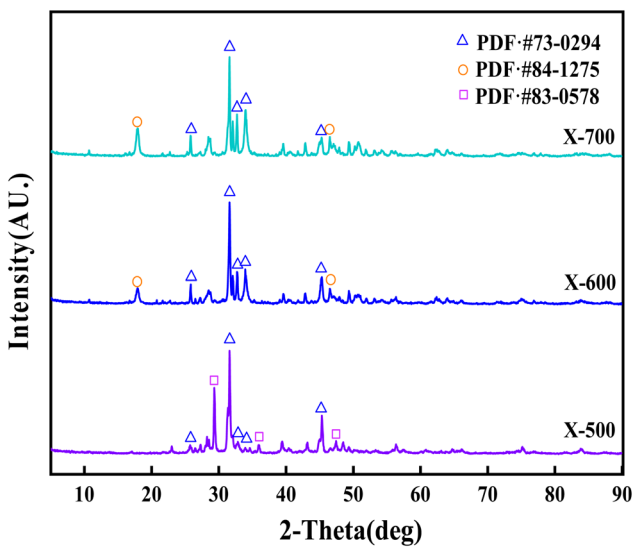

Fig. 4 XRD patterns of X-500, 600, and 700.

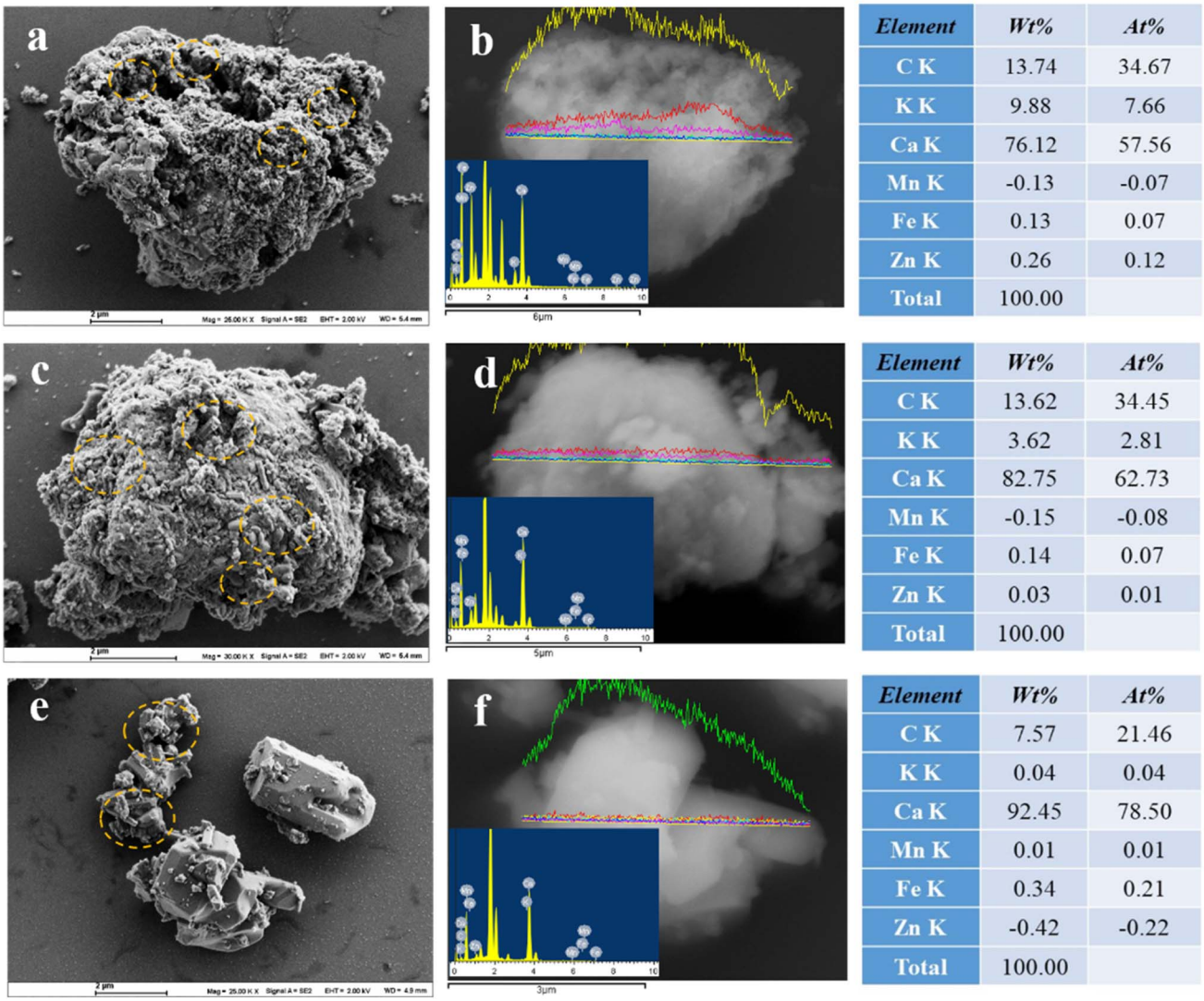

Element	Wt%	At%
C K	13.74	34.67
K K	9.88	7.66
Ca K	76.12	57.56
Mn K	-0.13	-0.07
Fe K	0.13	0.07
Zn K	0.26	0.12
Total	100.00	

Element	Wt%	At%
C K	13.62	34.45
K K	3.62	2.81
Ca K	82.75	62.73
Mn K	-0.15	-0.08
Fe K	0.14	0.07
Zn K	0.03	0.01
Total	100.00	

Element	Wt%	At%
C K	7.57	21.46
K K	0.04	0.04
Ca K	92.45	78.50
Mn K	0.01	0.01
Fe K	0.34	0.21
Zn K	-0.42	-0.22
Total	100.00	

Fig. 5 SEM and EDS images of X-500, 600, and 700 ((a and b) X-500; (c and d) X-600; (e and f) X-700).

this, and the content of $Ca(OH)_2$ in the catalyst component increases with the calcination temperature of the catalyst (Fig. 4).

Fig. 5 shows the SEM and EDS images of all the X catalysts. As shown in Fig. 5a, c and e, as the calcination temperature of the catalyst increases, the morphology of the catalyst changes from disorder to order. The cylindrical and regular polyhedral particles in the morphology gradually increase; this phenomenon indicates that an appropriate increase in temperature is beneficial for the formation of an ordered morphology of the prepared catalyst. Combined with EDS analysis results, it is evident that the element content of the catalyst changes with the calcination temperature. From these results, it can be seen that with the increase in temperature, the relative content of shrimp shell derived $Ca(OH)_2$ is increased. Specifically, the content of C and K elements gradually decreases, while the content of the Ca element continues to increase, and the changes in the contents of other elements are not obvious. The catalytic activity of the X catalyst is attributed to the presence of metals in the form of oxides, hydroxides, and salts; in other words, the components here gradually change from multiple complexes to simple. Additionally, the gradual ordering of the morphology positively affects the catalyst's activity.

The pore structure and characteristics of the X-500, 600, and 700 catalysts were examined by using N_2 adsorption–desorption isotherms, and the adsorption–desorption curves of the catalyst are depicted in Fig. 6. All the catalysts exhibited type-II isotherm curves, indicating that the pore structure is not obvious; this further illustrates that the increase in carbonization temperature does not play a positive role in the pore structure of this material, which indicates that the content of C may be beneficial for constructing the pore structure of the material.

3.2 Characterization and analysis of PET degradation products

The yield of BHET enabled the determination that the X-700 catalyst exhibited the most favorable activity (Fig. S2†). Additionally, the influence range of various factors in the degradation process of PET was identified (Fig. S3†). This information

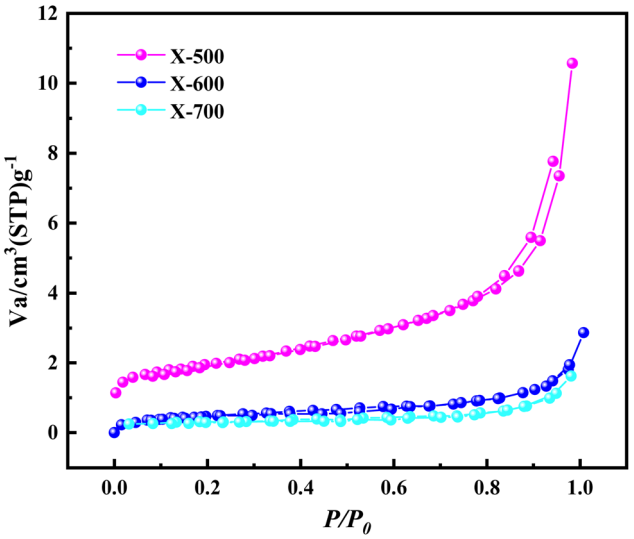

Fig. 6 N_2 adsorption–desorption isotherms of X-500, 600, and 700 catalysts.

was utilized to establish a response surface, which was employed to optimize the experimental process. The degradation products were characterized by FT-IR, DSC, and ^{1}H-NMR. FT-IR analysis preliminarily confirmed that the functional group structure of the product was consistent with BHET. DSC analysis determined that the depolymerized product did not contain oligomers and had a melting point close to the theoretical value of BHET. The ^{1}H-NMR analysis determined the position of the hydrogen atoms in the product. Based on the above characterization results, it was determined that the separated degradation product is highly pure BHET. (The analysis is shown in Fig. S4–S6 of the ESI†).

3.3 Optimization of the RSM for PET degradation

The RSM model employs the maximum BHET yield as the objective, with the optimization of reaction parameters conducted within the reference range defined by the independent variable level factors; the cross-relationship between different single factors was explored using the Box–Behnken design of the response surface. The RSM's 3D diagram displays the response values of the model under different conditions. If there is a bulge in the figure, it indicates a significant interaction between the two variables. Fig. 7 illustrates the influence of different factors on the BHET yield. In the 3D surface diagram, as shown in Fig. 7c, e and f, clear protrusions are visible, indicating a significant response relationship between the amount of catalyst and the three factors of EG dosage, alcoholysis time, and alcoholysis temperature. This is consistent with the maximum *F*-value of *D* in Table S2 in the ESI,† which confirms that the amount of EG has the greatest impact on the response surface. The response surface model was analyzed using Design-Expert software. The optimal experimental conditions were determined to be an alcoholysis temperature of 193 °C, an alcoholysis time of 3.6 h, the dosage of X-700 is 0.5%, and 13.9 ml EG. The aforementioned conditions led to a BHET yield

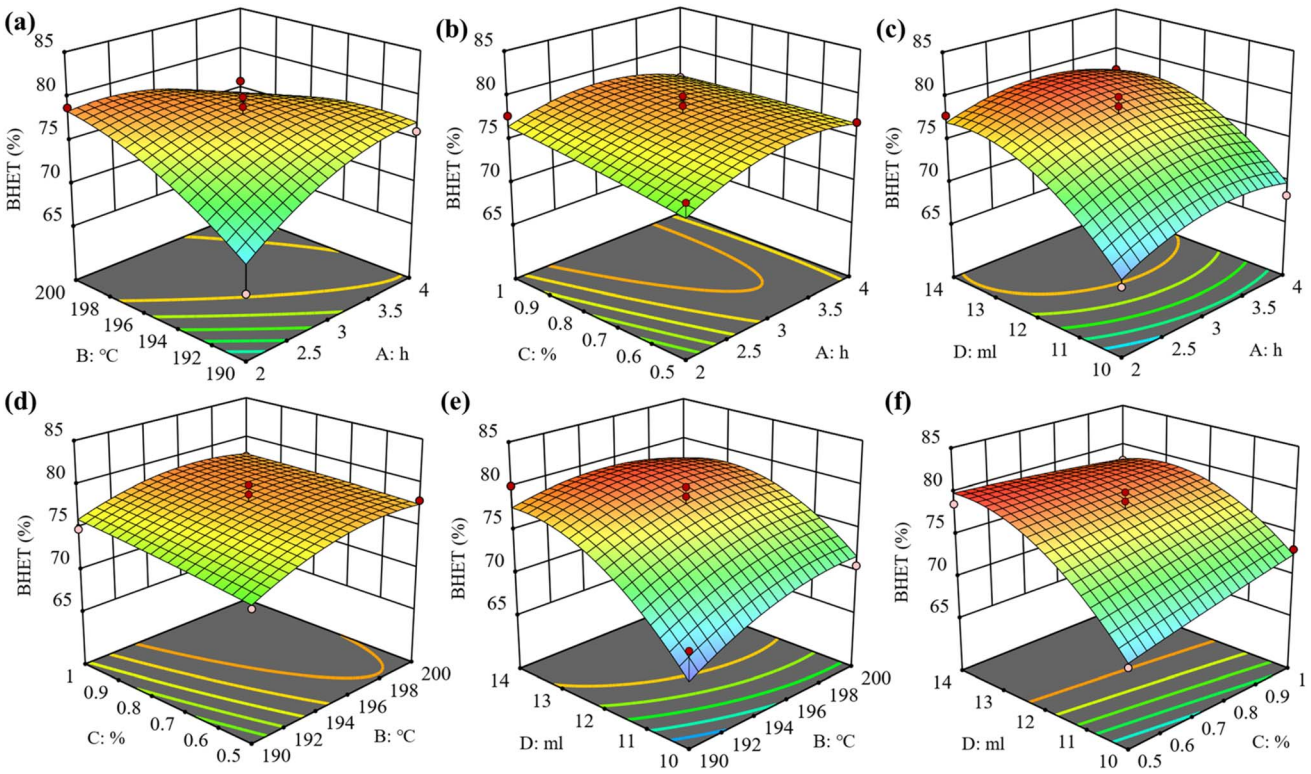

Fig. 7 Diagram of RSM between the various factors. (a): time and temperature; (b): time and catalyst dosage; (c): time and EG volume; (d): temperature and catalyst dosage; (e): temperature and EG volume; (f): catalyst dosage and EG volume.

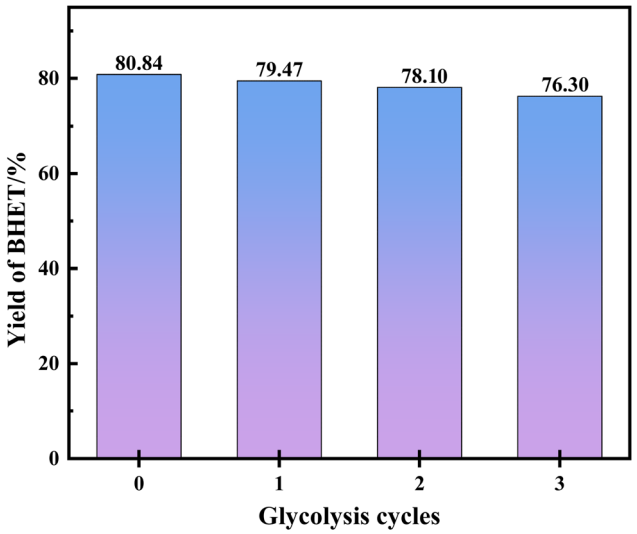

Fig. 8 Recycling of EG and the catalyst. T = 193 °C, time = 3.6 h, cat. = 0.5%, EG = 13.9 ml.

of 80.84% following the repetition of the experiment on three separate occasions, which closely matched the predicted yield of 80.05% with a residual of only 0.79%. This confirms the accuracy of the model's prediction. To further verify the reliability of the RSM model, a comparison was conducted between the predicted and actual BHET yield values, as illustrated in Fig. S7.† The results demonstrated a strong correlation between the two, indicating that the predicted values of the model are highly reliable.

3.4 Reusability of the catalyst

Furthermore, the recycling performance of the catalyst in the green degradation experiment was investigated by increasing the PET substrate amount by 2 times (6.0 g of PET) and the results are shown in Fig. 8. It was found that the yield of BHET could still reach 76.30% after three cycles. Of course, this phenomenon does not mean that it is all caused by the decrease in the activity of the catalyst, and both the dissolution of BHET in EG and the loss in the crystallization process can lead to a decrease in the yield of BHET. The analysis in Table S2 in the ESI† revealed that the amount of EG has the most pronounced impact on the system. However, due to considerations of cost, the loss of BHET dissolved in EG, and the dilution of the concentration of the catalyst brought about by the amount of EG, an appropriate increase in the amount of EG plays a beneficial role. It is therefore of particular importance to control the optimal experimental conditions obtained by model optimization.

3.5 Comparison of the catalytic performance

Fig. 9 shows that comparison of the catalytic activity of different catalysts for glycolysis of PET. It can be found that X-700 has higher catalytic performance in PET alcoholysis, and needs a smaller dosage of catalyst and mass ratio of EG/PET; this presents a favorable context for the large-scale implementation of X-700. This shows that the catalyst prepared by using biomass waste as a precursor has shown good performance in the high value-added utilization of waste PET.

3.6 The possible mechanism of the glycolysis of PET

The X-700 catalyst is composed of several metal elements, including Ca, K, Fe, and Mn, with Ca being the main component. The synergistic interaction between these metals during the catalytic process significantly enhances the catalytic activity of Ca-based catalysts in the PET depolymerization process. This finding is consistent with the results presented in the previous section on catalyst characterization. The primary process for achieving efficient PET depolymerization with the X-700 catalyst is as follows (Fig. 10): the catalyst is activated when the solvent glycol molecules combine with the metal center of X-700, resulting in the formation of the M–$C_2H_6O_2$ structure. Upon

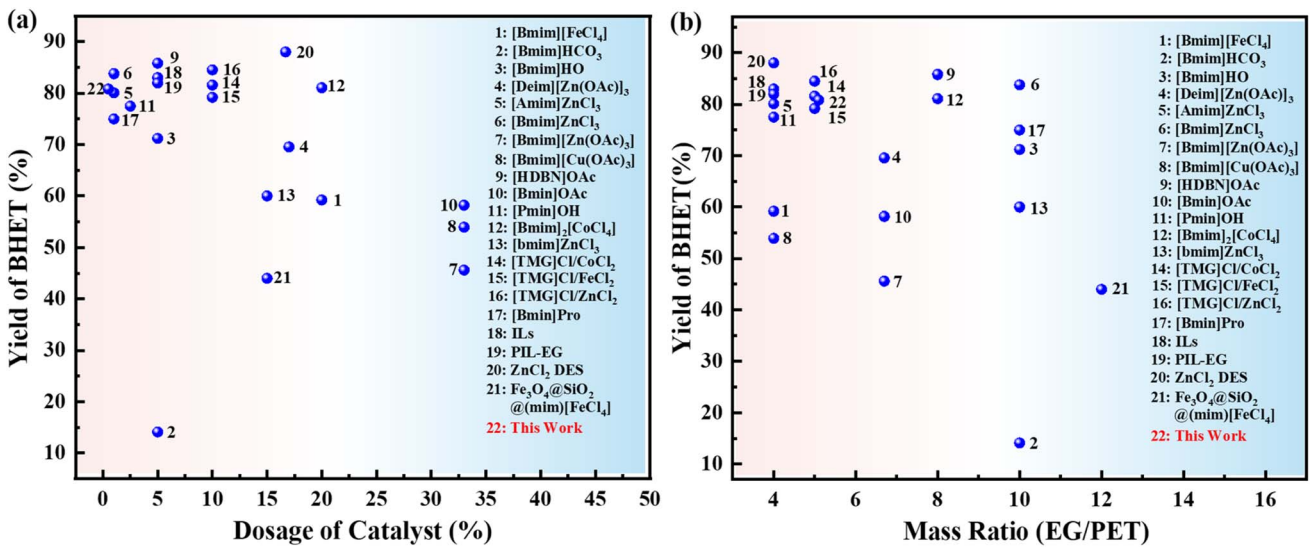

Fig. 9 Comparison of catalytic activity of different catalysts in PET alcoholysis.

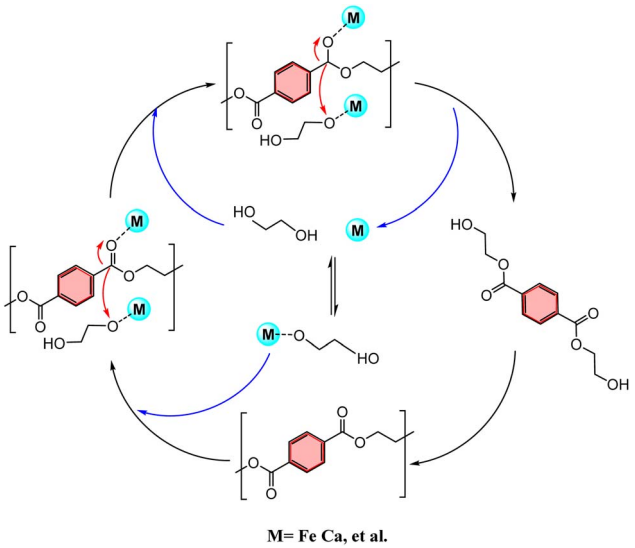

Fig. 10 Mechanism prediction of PET degradation catalyzed by X-700.

activation, the metal center M of the X-700 catalyst contains empty orbitals, making it a Lewis acid catalyst. It then attacks the O═C of O═C–O in the PET molecule and accepts the lone electron pair of O in O═C, resulting in the cleavage of O═C–O. The cleaved O═C then combines with the –OH of the solvent ethylene glycol to form a new O═C–O, leading to a decrease in molecular weight and the production of PET with a low degree of polymerization (L-PET). The degradation of PET to BHET is achieved through this reaction process.

4 Conclusion

In conclusion, this work provides a research idea of "treating waste with waste"; this concept is an active response to the notion of a "green, economic" chemistry. The X-700 catalyst prepared by using kitchen waste shrimp shells as precursors, effectively catalyzes the glycolysis of waste PET into high value-added monomers, achieving high conversion of PET (100%) and high yield of BHET (80.84%) in a short reaction time and with a small catalyst and EG dosage; the results of the experimental investigation demonstrate that the BBD design method facilitates the simplification of the degradation process of PET. This has the potential to result in cost savings during the commercialization process. The catalyst preparation process described is simple, low-cost, and highly effective. The optimal reaction conditions were obtained through response surface design method optimization. These findings provide valuable insights for the design of bio-based catalysts and the treatment of waste resources.

Abbreviations

PET	Polyethylene terephthalate
BHET	Bis(2-hydroxyethyl)terephthalate
RSM	Response surface methodology
DOE	Design of experiments
ANOVA	Analysis of variance
EG	Ethylene glycol
^{1}H-NMR	Nuclear magnetic resonance
SEM	Scanning electron microscopy
EDS	Energy dispersive X-ray spectroscopy
FT-IR	Fourier transform infrared spectroscopy
DSC	Differential scanning calorimetry
BET	Brunauer–Emmett–Teller

Data availability

The data are not publicly available due to their containing information that could compromise the privacy of research participants.

Conflicts of interest

The authors declare that they have no known competing financial interests or personal relationships that could have appeared to influence the work reported in this paper.

Acknowledgements

The authors assert that this work was completed without financial support and without acknowledging any funding or institutional affiliations. We thank all authors for their contributions to this paper.

References

1 C. Ke, X. Pan, P. Wan, Z. Jiang and J. Zhao, *Sustain. Prod. Consum.*, 2023, **41**, 348–361.
2 W. Qian, X. Ji, P. Xu and L. Wang, *Text. Res. J.*, 2021, **91**, 2468–2475.
3 J. Lee, T. Lee, Y. F. Tsang, J.-I. Oh and E. E. Kwon, *Energy Convers.*, 2017, **148**, 456–460.
4 J. Chu, Y. Cai, C. Li, X. Wang, Q. Liu and M. He, *Waste Manage.*, 2021, **124**, 273–282.
5 R. Wen, G. Shen, Y. Yu, S. Xu, J. Wei, Y. Huo and S. Jiang, *RSC Adv.*, 2023, **13**, 17166–17178.
6 Z. Wang, Y. Jin, Y. Wang, Z. Tang, S. Wang, G. Xiao and H. Su, *ACS Sustainable Chem. Eng.*, 2022, **10**, 7965–7973.
7 X. Zhou, C. Wang, C. Fang, R. Yu, Y. Li and W. Lei, *Waste Manage.*, 2019, **85**, 164–174.
8 Z. Jiang, D. Yan, J. Xin, F. Li, M. Guo, Q. Zhou, J. Xu, Y. Hu and X. Lu, *Polym. Degrad. Stab.*, 2022, **199**, 109905.
9 J. Tang, X. Meng, X. Cheng, Q. Zhu, D. Yan, Y. Zhang, X. Lu, C. Shi and X. Liu, *Ind. Eng. Chem. Res.*, 2023, **62**, 4917–4927.
10 J. Liang, J. Fu, H. Lin, J. Chen, S. Peng, Y. Sun, Y. Xu and S. Kang, *J. Ind. Eng. Chem.*, 2024, **132**, 578–587.
11 A. Mittal, R. K. Soni, K. Dutt and S. Singh, *J. Hazard. Mater.*, 2010, **178**, 390–396.
12 H. Abedsoltan, *Polym. Eng. Sci.*, 2023, **63**, 2651–2674.
13 P. Pereira, P. E. Savage and C. W. Pester, *Green Chem.*, 2024, **26**, 1964–1974.

14 Y. Yu, G. Shen, T. J. Xu, R. Wen, Y. C. Qiao, R. C. Cheng and Y. Huo, *RSC Adv.*, 2023, **13**, 36337–36345.
15 S. Mohammadi and M. Enayati, *Polym. Degrad. Stab.*, 2022, **206**, 110180.
16 L. Bartolome, M. Imran, K. G. Lee, A. Sangalang, J. K. Ahn and D. H. Kim, *Green Chem.*, 2014, **16**, 279–286.
17 J. S. Bin, J. J. Min, S. S. Gyu, P. S. Hwa, K. G. Lee and C. B. Gill, *Mater. Today Commun.*, 2020, **26**, 101857.
18 W. Rui, W. Tianlin, Y. Guangren and C. Xiaochun, *Polym. Degrad. Stab.*, 2021, **183**, 109463.
19 X. Zhou, X. Lu, Q. Wang, M. Zhu and Z. Li, *Pure Appl. Chem.*, 2012, **84**, 789–801.
20 S. Javed, D. Ropel and D. Vogt, *Green Chem.*, 2023, **25**, 1442–1452.
21 N. Yan and X. Chen, *Nature*, 2015, **524**, 155–157.
22 X. Chen, S. Song, H. Y. Li, G. Gözaydin and N. Yan, *Acc. Chem. Res.*, 2021, **54**, 1711–1722.
23 Y. Kim, M. Kim, J. Hwang, E. Im and G. D. Moon, *Polymers*, 2022, **14**, 656.
24 Z. Laldinpuii, S. Lalhmangaihzuala, Z. Pachuau and K. Vanlaldinpuia, *Waste Manage.*, 2021, **126**, 1–10.
25 I. Yunita, S. Putisompon, P. Chumkaeo, T. Poonsawat and E. Somsook, *Chem. Pap.*, 2019, **73**, 1547–1560.
26 M. Feng, J. P. Yan, B. He, X. Y. Chen and J. Sun, *Int. J. Biol. Macromol.*, 2021, **193**, 347–357.
27 F. Gao, Y. Q. Xie, Y. H. Zang, G. Zhou, J. Y. Qu and M. B. Wu, *New Carbon Mater.*, 2022, **37**, 750–751.
28 P. Zhu, Z. J. Gu, S. Hong and H. L. Lian, *Carbohydr. Polym.*, 2017, **177**, 217–223.
29 L. J. He and H. Y. Du, *J. Food Compos. Anal.*, 2023, **118**, 105200.
30 B. Joseph, R. M. Sam, P. Balakrishnan, H. J. Maria, S. Gopi, T. Volova, S. C. M. Fernandes and S. Thomas, *Polymers*, 2020, **12**, 1664.
31 F. Yang, M. L. Cai, W. Chen and Z. W. Bai, *Carbohydr. Polym.*, 2019, **204**, 238–246.
32 Y. J. Gao, X. Chen, J. G. Zhang and N. Yan, *ChemPlusChem*, 2015, **80**, 1556–1564.
33 R. Wen, G. Shen, Y. Yu, J. Zhu, S. Xu, J. Wei and Y. Huo, *Environ. Sci. Pollut. Res.*, 2024, **31**, 33443–33453.
34 R. Wen, G. Shen, J. Zhai, L. Meng and Y. Bai, *New J. Chem.*, 2023, **47**, 14646–14655.
35 H. S. Kusuma, A. Ansori, S. Wibowo, D. S. Bhuana and M. Mahfud, *Korean Chem. Eng. Res.*, 2018, **56**, 435–440.